

# Meta-learning with GANs for anomaly detection, with deployment in high-speed rail inspection system

Haoyang Cao<sup>\*</sup>      Xin Guo<sup>†</sup>      Guan Wang<sup>‡</sup>

February 14, 2022

## Abstract

Anomaly detection has been an active research area with a wide range of potential applications. Key challenges for anomaly detection in the AI era with big data include lack of prior knowledge of potential anomaly types, highly complex and noisy background in input data, scarce abnormal samples, and imbalanced training dataset. In this work, we propose a meta-learning framework for anomaly detection to deal with these issues. Within this framework, we incorporate the idea of generative adversarial networks (GANs) with appropriate choices of loss functions including structural similarity index measure (SSIM). Experiments with limited labeled data for high-speed rail inspection demonstrate that our meta-learning framework is sharp and robust in identifying anomalies. Our framework has been deployed in five high-speed railways of China since 2021: it has reduced more than 99.7% workload and saved 96.7% inspection time.

## 1 Introduction

Anomaly detection has been an active research area with a wide range of potential applications such as fraud detection in health insurance, cyber attacks, and military surveillance [3]. The goal of anomaly detection is to identify abnormal input data that does not conform to a given data description.

**Motivating example of anomaly detection.** High-speed rail inspection is one example of anomaly detection that embodies the key challenges in the AI era. In a high-speed rail system, identification and removal of foreign abnormal objects is critical for the safety of railway operation. However, there are limited number of inspectors in contrast to hundreds

---

<sup>\*</sup>Centre de Mathématiques Appliquées, École Polytechnique, Route de Saclay, 91128, Palaiseau Cedex, France, haoyang.cao@polytechnique.edu

<sup>†</sup>Department of IEOR, University of California, Berkeley, Berkeley, California, 94709, United States, xinguo@berkeley.edu

<sup>‡</sup>Tsinghua-Berkeley Shenzhen Institute, Shenzhen, P. R. China, wangguan17@mails.tsinghua.edu.cn

of thousands of miles of railway to inspect. Current practice in China, for instance, is first to take photos of the track and its vicinity using a camera on a moving train, and then to manually inspect potential abnormal objects from the photos. This manual inspection process is tedious and prone to human errors: for each rail line there are over tens of thousands of images taken each week; and for each image it takes from 30 seconds to a minute for each inspector to check and record. This amounts to hundreds of working hours for each line, even with the aid of industrial high-definition cameras to digitize track status.

Speedy and accurate identification of anomaly for high-speed rail is a formidable task, for several reasons. First, climatic and geographic changes lead to different distributions of images collected from the rail lines, and the background of images are highly noisy, diverse, and complex. Second, all kinds of foreign objects can fall onto or near the track. Therefore, it is infeasible to know *a priori* all anomaly types. Third, among all potential anomaly types, those captured by inspection photos are extremely limited and such instances are negligibly infrequent. Thus data are highly imbalanced (see Columns (A) and (B) in Table 1a). Finally, labeled data are extremely limited, as labeling hundreds of thousands of images is labor intensive.

**Main challenges.** The example of high-speed rail anomaly detection highlights some of main challenges for the most formidable anomaly detection problems, including

- Highly diverse, complex and noisy background in input data;
- No prior knowledge of anomaly types;
- Exceedingly imbalanced training dataset, with very limited or no abnormal sample data.

**Existing approaches for anomaly detection.** Early works on anomaly detection [38] adopt classification techniques, including neural networks, Bayesian networks, support vector machine, and nearest neighbor [3]. These traditional supervised-learning methods face the overfitting issue when abnormal samples are limited and the training dataset is imbalanced. Alternatively, unsupervised learning approaches such as clustering-based anomaly detection [38] have been developed. These methodologies, however, rely on the crucial assumption that normal data lie close to their closest cluster centroid whereas anomalies are far away from those clusters. Moreover, techniques such as k-means clustering can be negatively impacted by outliers and are not suitable for identifying clusters with irregular shapes. Additionally, semi-supervised deep learning techniques have been proposed for anomaly detection, including long-short term memory [17], convolutional neural network [20], autoencoder [16], deep neural network [15], spatial transformer network [5], adversarial autoencoder [27], variational autoencoder [40], and generative adversarial networks (GANs) ([4, 26, 36]. These models learn patterns and features of the normal data distribution, and produce outstanding performance for detecting anomalies. Additionally, *model-agnostic meta-learning* framework has been adopted to solve multiple anomaly detection tasks ([24, 43, 46]). However, all these techniques require refined and simple backgrounds against which abnormal samples are distinctive.

**Previous works on railway track inspection.** In [11], end-to-end deep convolutional neural networks (DCNN) are adopted to inspect fatigue cracks of timber using material classification and semantic segmentation. The work of [12] adopts the histogram of oriented gradients features and a combination of linear SVM classifiers to detect fasteners and ties of the track. Similar work has been done in [7] to detect partially worn and completely missing fasteners using probabilistic topic model. [19] designs an R-CNN network for the insulator inspection. All techniques from these works for anomaly detection belong to the category of supervised learning and require abundant labeled data with known anomaly types.

**Our approach.** The goal of our study is to develop an anomaly detection framework that requires little-to-no labeled training data which may be highly imbalanced and to produce accurate detection regardless of the image backgrounds.

- To deal with different distributions of samples images, we propose and develop a *meta-learning framework* to solve *multiple tasks* of anomaly detection.
- In the meta-learning framework, the meta objective is designed to restore images and to correct any possible anomalies, and the individual tasks are binary classifications for collected images. In the meta objective, we incorporate the idea of generative adversarial networks (GANs) [13] to ensure a credible reconstruction of target images from input; we also adopt the structural similarity index measure (SSIM) to enhance the identification of the anomalies. This addition of GANs and SSIM resolves the issue of unlabeled data.
- We design neural network architectures that are tailored for this meta-learning framework.

**Our results.** We first experiment our meta-learning framework with limited labeled data to test its accuracy and robustness and eventually deploy it within the high-speed rail inspection system with no labeled data.

The experiment demonstrates superb performance of this meta-learning framework: with both limited labeled data and limited known anomaly samples, it rarely misses any anomalies that were previously detected by human inspectors and it is robust with respect to the reduction in the number of labeled samples. Moreover, it can detect several folds more anomalies than human inspectors.

Our framework has been deployed in five high-speed railways of China since 2021. Without any prior labeled data, it has detected several times more new anomalies than human inspectors; it has reduced the workload of inspecting millions of images to simply double-checking hundreds of identified images, a workload reduction of over 99.7%; and it takes less than two days for anomaly detection, instead of several months for purely manual inspection, 96.7% inspection time saved.

## 2 Technical Components for High-Speed Rail Anomaly Detection

### 2.1 Review

**Meta learning.** As reviewed in [18], meta-learning is a broad learning paradigm. Combined with deep neural networks and reinforcement learning techniques, meta learning has gained substantial attention in model-agnostic learning [9], online learning [8], memory-augmented neural networks [35] and latent-embedded optimization [34].

In contrast to conventional machine learning where the learning tasks are often solved independently, meta-learning leverages the experience of multiple learning episodes. Under a multi-task scenario, a meta-learning framework typically specifies a set of task-independent features among all tasks. On top of these tasks, a different optimization problem is employed with respect to these task-independent features. This optimization is often referred to as the *meta objective* and is for improving the learning outcome of these individual tasks.

A typical meta-learning framework across  $K \in \mathbb{N}$  various tasks can be seen as the following bi-level optimization problem,

$$\min_{\omega \in \Omega} \sum_{i=1}^K \mathcal{L}_{\text{meta}}(\theta_i^*(\omega), \omega), \quad (1)$$

where for  $i = 1, \dots, K$ ,  $\theta_i^*(\omega)$  is defined as

$$\theta_i^*(\omega) \in \arg \min_{\theta \in \Theta_i} \mathcal{L}_i(\theta, \omega), \quad \forall \omega \in \Omega. \quad (2)$$

Here, the outer optimization Equation (1) with loss function  $\mathcal{L}_{\text{meta}}$  is seen as the meta objective, and the inner optimization Equation (2) with loss function  $\mathcal{L}_i$  is seen as the task-specific objective. The set  $\Omega \subset \mathbb{R}^k$  contains all possible task-independent parameter  $\omega$  shared across all  $K$  tasks.  $\Theta_i \subset \mathbb{R}^{d_i}$  denotes the set of task  $i$ -specific parameters  $\theta$ , for  $i = 1, \dots, K$ . Loss functions  $\mathcal{L}_{\text{meta}}$  and  $\mathcal{L}_i$ 's are to optimize task-independent parameter  $\omega$  and task-specific parameters  $\theta$ , respectively.

Proposing meta-learning framework for anomaly detection is to overcome the obstacle in the traditional classification formulation with unlabeled data.

**GANs.** Generative adversarial networks (GANs), introduced in [13], belong to the class of generative models. Since the inception, GANs have enjoyed tremendous empirical successes in high resolution image generation [6, 31], text-to-image synthesis [32], video generation [39], semantic segmentation [25], and abstract reasoning diagram generation [10].

The key idea behind GANs is to interpret the process of generative modeling as a competing game between two neural networks: a generator neural network  $G_{\omega_G}$  with parameters  $\omega_G$  and a discriminator neural network  $D_{\omega_D}$  with parameters  $\omega_D$ . The generator network  $G_{\omega_G}$  attempts to fool the discriminator network by mapping random noise  $Z$  from a latent space  $\mathcal{Z}$  into the sample space  $\mathcal{X}$ , while the discriminator network  $D_{\omega_D}$  tries to identify whether an input sample is faked or true. A vanilla formulation in [13] is a minimax problem,

$$\min_{\omega_G} \max_{\omega_D} \mathbb{E}[\log(D_{\omega_D}(X)) + \log(1 - D_{\omega_D}(G_{\omega_G}(Z)))]. \quad (3)$$

Other frameworks of GANs include f-GAN [28], Wasserstein GAN [1], relaxed-Wasserstein GAN [14], and a survey paper [2].

Incorporating GANs into the meta objective for anomaly detection is to ensure a credible production of the target image from the input image.

**SSIM** Structural similarity index measure is a perception-based model widely used in the field of image reconstruction [45], object detection [30], super-resolution [44], and image deblurring [21].

The key idea behind SSIM is to perceive image degradation as structural changes in luminance and contrast. Structural similarity comparison is based on the notion that pixels have strong inter-dependence, especially when they are spatially close and these dependencies carry important visual information about the structure of the objects [41]. Luminance comparison comes from the experience that image distortions tend to be less visible in bright regions, whereas contrast comparison is built on the intuition that distortions become less visible where there is significant amount of activity or texture in the image.

For two sample images  $Y, Y' \in \mathbb{R}^{w \times h \times 3}$  of width  $w \in \mathbb{N}$  and height  $h \in \mathbb{N}$ , the SSIM loss [42] is given by

$$L_{\text{SSIM}}^{\alpha, \beta, \gamma}(Y, Y') = l(Y, Y')^\alpha \cdot c(Y, Y')^\beta \cdot s(Y, Y')^\gamma, \quad (4)$$

where  $\alpha, \beta, \gamma$  are constants and the functions  $l(Y, Y')$ ,  $c(Y, Y')$  and  $s(Y, Y')$  represent image illumination comparison, contrast comparison, and structural similarity comparison between  $Y$  and  $Y'$ , respectively, and

$$\begin{aligned} l(Y, Y') &= \frac{\sum_{i=1}^w \sum_{j=1}^h \sum_{k=1}^3 \frac{2\mathbb{E}_Y[Y_{ijk}]\mathbb{E}_{Y'}[Y'_{ijk}] + c_1}{\mathbb{E}_Y[Y_{ijk}]^2 + \mathbb{E}_{Y'}[Y'_{ijk}]^2 + c_1}}{w \times h \times 3}, \\ c(Y, Y') &= \frac{\sum_{i=1}^w \sum_{j=1}^h \sum_{k=1}^3 \frac{2\text{Cov}_{Y, Y'}(Y_{ijk}, Y'_{ijk}) + c_2}{\text{Var}_Y(Y_{ijk}) + \text{Var}_{Y'}(Y'_{ijk}) + c_2}}{w \times h \times 3}, \\ s(Y, Y') &= \frac{\sum_{i=1}^w \sum_{j=1}^h \sum_{k=1}^3 \frac{\text{Cov}_{Y, Y'}(Y_{ijk}, Y'_{ijk}) + c_3}{\text{Var}_Y(Y_{ijk})\text{Var}_{Y'}(Y'_{ijk}) + c_3}}{w \times h \times 3}, \end{aligned} \quad (5)$$

with  $c_1, c_2$  and  $c_3$  some constants.

Including SSIM loss into the meta-learning framework for anomaly detection is to emphasize the contrast between input images (especially those containing abnormal areas) and their reconstructed version, and hence highlight the anomaly correction step in the meta objective.

## 2.2 Meta-learning framework for anomaly detection

**Notation.** Since the sample dataset consists of image data, we use  $\mathcal{X} \subset \mathbb{R}^{w \times h \times 3}$  to denote the sample space, where  $w$  and  $h$  are the width and the height of sample images. For any sample image  $X \in \mathcal{X}$ , for instance an image of a railway track segment, we pair it with a target image  $Y \in \mathcal{X}$  which is a clean version of  $X$  without any anomaly, and denote the pair as  $(X, Y)$ .

**Meta objective.** The first building block is a generative model to reconstruct an image of  $Y$  via a mapping  $G : \mathcal{X} \times \mathcal{Z} \rightarrow \mathcal{X}$ , where  $\mathcal{Z}$  is a latent space. That is,  $G$  takes a sample image  $X \in \mathcal{X}$  and a latent random variable  $Z \in \mathcal{Z}$  as inputs, and produces a corrected version of  $X$ , namely  $G(X, Z)$ , so that the generated pair  $(X, G(X, Z))$  resembles the pair  $(X, Y)$  from the training dataset.

The second building block is to choose appropriate measures between the generated images and the original ones, including

1. the divergence between the distribution of  $(X, G(X, Z))$  and that of  $(X, Y)$ ;
2. the perceptual difference between  $G(X, Z)$  and  $Y$ .

To handle the distributional divergence, we will adopt GANs [13] and introduce discriminator  $D : \mathcal{X} \times \mathcal{X} \rightarrow [0, 1]$  to estimate the Jensen–Shannon divergence between the joint distribution of  $(X, G(X, Z))$  and that of  $(X, Y)$ . To measure the distance between images  $G(X, Z)$  and  $Y$ , we will adopt both the  $L_2$  loss and structural similarity loss (SSIM). Combined, the meta objective of anomaly detection is formulated as the following minimax model,

$$\min_{\omega_G} \max_{\omega_D} \mathcal{L}_{\text{meta}}(G_{\omega_G}, D_{\omega_D}). \quad (6)$$

Here,  $G_{\omega_G} : \mathcal{X} \times \mathcal{Z} \rightarrow \mathcal{X}$  and  $D_{\omega_D} : \mathcal{X} \times \mathcal{X} \rightarrow [0, 1]$  denote two parametrized neural networks approximating  $G$  and  $D$ , respectively. Their corresponding parameters,  $\omega_G$  and  $\omega_D$ , constitute the task-independent parameter  $\omega = (\omega_G, \omega_D) \in \Omega \subset \mathbb{R}^k$  of the meta objective; here the dimension  $k$  denotes the number of parameters to train in both networks  $G_{\omega_G}$  and  $D_{\omega_D}$ . Moreover, the objective function  $\mathcal{L}_{\text{meta}}$  is modified from GANs’ objective and defined as

$$\begin{aligned} \mathcal{L}_{\text{meta}}(G_{\omega_G}, D_{\omega_D}) &= V_{\text{GAN}}(G_{\omega_G}, D_{\omega_D}) \\ &\quad + w_1 V_{L_2}(G_{\omega_G}) - w_2 V_{\text{SSIM}}(G_{\omega_G}). \end{aligned} \quad (7)$$

Here,  $V_{\text{GAN}}$  takes the form of the loss function for vanilla GANs (3) such that

$$\begin{aligned} V_{\text{GAN}}(G_{\omega_G}, D_{\omega_D}) &= \mathbb{E}_{X,Y} \log D_{\omega_D}(X, Y) \\ &\quad + \mathbb{E}_{X,Z} \log [1 - D_{\omega_D}(X, G_{\omega_G}(X, Z))], \end{aligned}$$

$V_{L_2}$  and  $V_{\text{SSIM}}$  are given by

$$V_{L_2}(G_{\omega_G}) = \mathbb{E} \|Y - G_{\omega_G}(X, Z)\|^2,$$

and

$$\begin{aligned} V_{\text{SSIM}}(G_{\omega_G}) &= L_{\text{SSIM}}^{1,1,1}(Y, G_{\omega_G}(X, Z)) = l(Y, G_{\omega_G}(X, Z)) \\ &\quad \cdot c(Y, G_{\omega_G}(X, Z)) \cdot s(Y, G_{\omega_G}(X, Z)), \end{aligned}$$

where functions  $l(Y, Y')$ ,  $c(Y, Y')$  and  $s(Y, Y')$  represent image illumination comparison, contrast comparison, and structural similarity comparison of random samples  $Y, Y' \in \mathcal{X}$ , respectively, according to Equation (5).

Having  $V_{\text{GAN}}$  as part of the meta objective is to ensure a credible reproduction of the input image. It also differentiates our meta-learning framework for anomaly detection from conventional meta-learning models: instead of a pure minimization problem such as (1), our

meta objective (6) solves for a saddle point  $\omega^* = (\omega_G^*, \omega_D^*)$  of a minimax problem because of the composition of Equation (7); another noticeable difference is that our meta objective (6) does not depend on the results of individual tasks and it is due to the generative nature of  $G_{\omega_G}$ . In addition, to strengthen the correction ability of  $G_{\omega_G}$ ,  $V_{\text{GAN}}$  is enhanced on the generator side by adding  $L_2$  loss [29] and structural similarity (SSIM) loss [42].

**Task-specific objective.** For anomaly detection problem of complex backgrounds, we disintegrate it into multiple binary classification problems so that within each task, the input images are assume to follow the same distribution.

Previously in the meta objective, the goal is for the network  $G_{\omega_G}$  to restore input images and correct any possible anomalies. However,  $G_{\omega_G}$  itself will not determine the anomaly of the original image. After solving the meta objective and fix a task-independent parameter  $\omega = (\omega_G, \omega_D)$  from the minimax model, we now formulate the anomaly detection as a binary classification problem.

In particular, for any given task  $i = 1, \dots, K$  and the corresponding samples  $X^i$ , first its corrected sample  $\hat{X}^i(\omega) = G_{\omega_G}(X^i, Z)$  is construct. Then, the SSIM loss is computed for  $(X^i, \hat{X}^i(\omega))$  and with a predetermined threshold value  $\mu_0 > 0$ , one can assign a corresponding label  $\mathbf{1}_{X^i}\{\text{normal}\}$  and extract the appropriate classifier input  $f(X^i, \hat{X}^i(\omega))$  in a feature space  $\mathcal{Y}$ . A detailed labelling and feature extraction procedure can be found in Section 4. Let  $\theta_i \in \Omega_i \subset \mathbb{R}^{d_i}$  be the individual task parameter for the binary classifier  $p_{\theta_i} : \mathcal{Y} \rightarrow [0, 1]$  for task  $i$ . Here, the dimension  $d_i$  specifies the number of parameters to train in the classifier network, and  $p_{\theta_i}(f(X^i, \hat{X}^i(\omega)))$  is the probability of  $X^i$  being a normal image. Then the task-specific loss is given by cross-entropy value,

$$\begin{aligned} \mathcal{L}_i(\theta_i, \omega) = & -\mathbb{E}_{X^i, Z} \left[ \mathbf{1}_{X^i}\{\text{normal}\} p_{\theta_i} \left( f(X^i, \hat{X}^i(\omega)) \right) \right. \\ & \left. + (1 - \mathbf{1}_{X^i}\{\text{normal}\}) \left[ 1 - p_{\theta_i} \left( f(X^i, \hat{X}^i(\omega)) \right) \right] \right], \end{aligned} \quad (8)$$

and  $\theta_i(\omega) \in \arg \min_{\theta_i} \mathcal{L}_i(\theta_i, \omega)$ .

### 3 Network architectures for the meta-learning framework

Our meta-learning framework involves designing appropriate neural networks for both the minimax problem (6) as the meta objective and the classification problem (8) as the task-specific objective.

For the minimax problem (6), the network structure includes two neural networks  $G_{\omega_G}$  and  $D_{\omega_D}$ , as shown in Figure 1. The generator network  $G_{\omega_G}$  consists of an encoder, a decoder, and a direct link called U-NET structure [33] between them to enhance the information passage. More specifically, there are  $2n$  layers (for instance, in this paper  $n = 8$ ) in the network  $G_{\omega_G}$  with the encoder and the decoder each containing  $n$  layers. For  $i = 1, \dots, n$ , the output of the  $i$ -th layer in the encoder is passed to both the  $(i + 1)$ -th encoder layer

and the  $(n - i)$ -th decoder layer. The decoder then integrates this extra information from the encoder into the usual forward propagation through the decoder layers and generates normal images by removing possible anomalies. The discriminator network  $D_{\omega_D}$  is composed of a 5-layer convolution network [31], with its details shown in Figure 2. To better focus on local images, the network  $D_{\omega_D}$  uses the PatchGAN architecture [23], which has been proved effective in the classification of local classifiers instead of global classifiers. PatchGAN also reduces the number of parameters, thereby improving the training efficiency.

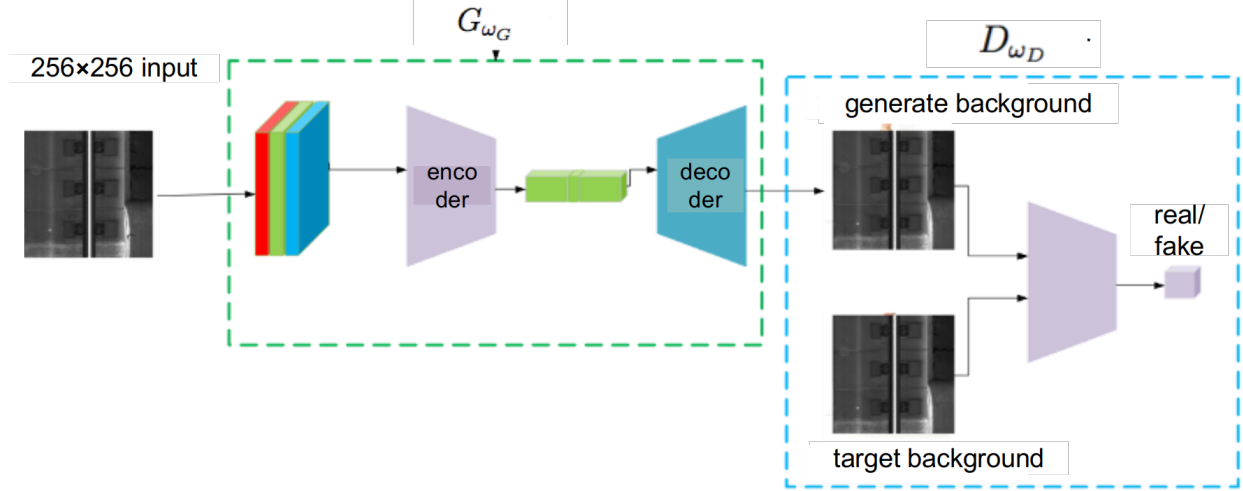


Figure 1: Network Structure for the Meta Objective

For the task-specific objective (8), the network adopted is the convolutional neural network (CNN) [22] and consists of the feature extractor and the decoder. The feature extractor has several convolutional layers and pooling layers. It captures basic features such as lines and corners in the first few layers and extracts more advanced features such as indicators of anomalies in the later layers. The extracted features are then fed into the decoder part. The decoder is a set of fully connected layers and uses extracted features to predict the target variable. In anomaly detection, the probability of an input image being anomaly is the target variable. We adopt a shallow CNN model with only four layers: two convolution layers and two fully-connected layers. To prevent overfitting, we add dropout layers [37] in the decoder part and the  $L^2$  regularization for the kernel of the fully connected layers.

## 4 Experiments on high-speed rail detection dataset

We apply our meta-learning framework to the railway detection dataset. The dataset contains nearly a million images collected from five high-speed rail lines in China (i.e., the number of individual tasks  $K = 5$ ). These images are not labeled and abnormal images can only be confirmed after manual verification from the detected samples. Foreign objects refer to objects that do not belong to the rail track itself. The most common ones are nails broken from the rail, stones, various types of garbage, and dead animals.

Columns (A) and (B) in Table 1a contain basic information of these five rail lines, where the *Total Number of Images* refers to the total number of images in each rail line, and the



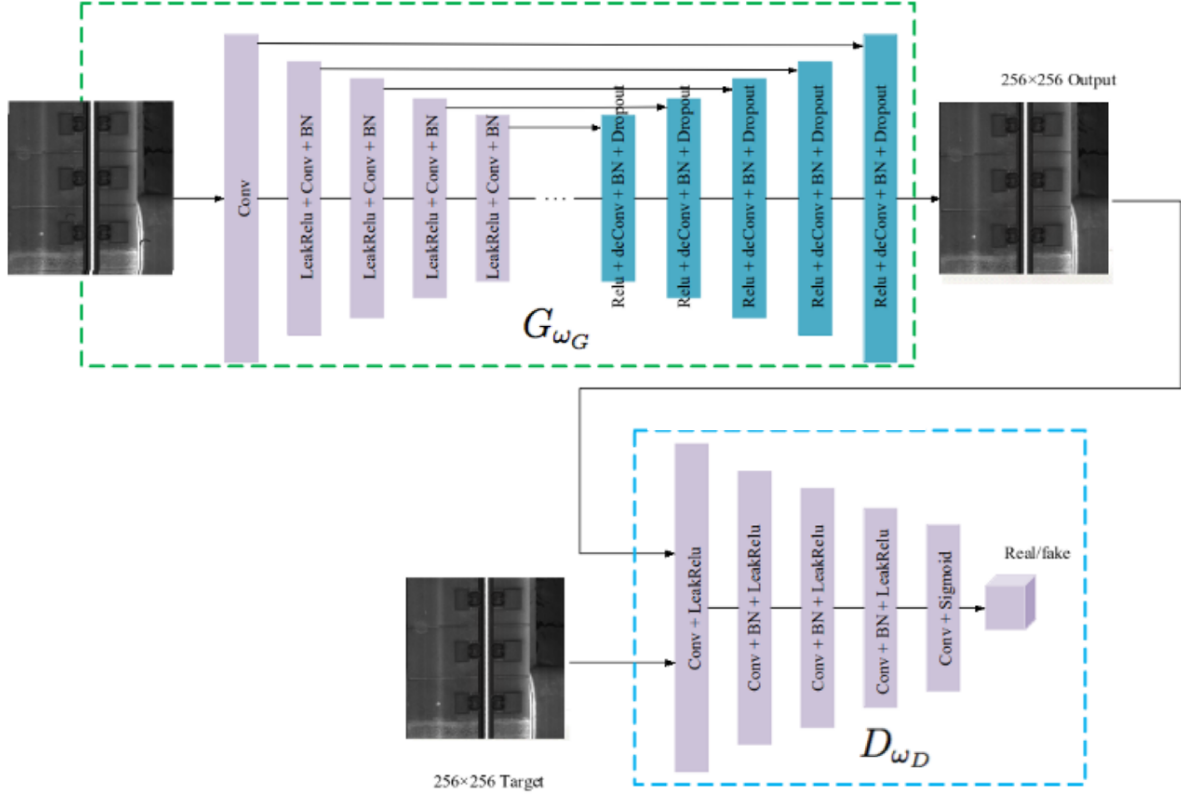


Figure 2: Details of Network Structure for the Meta Objective

*Official Anomaly Record* refers to the number of anomaly cases recorded by railway operation staff through regular inspections.

**Data pre-processing.** For data pre-processing, we synthesize abnormal samples by pasting images of commonly seen foreign objects onto images originally collected from the rail lines. If sizes of foreign objects are disproportionately small compared with the original images, we group two to fifteen such foreign objects when pasting. As a result, the complete set of training data  $\mathcal{X} \subset \mathbb{R}^{256 \times 256 \times 3}$  includes the original images as well as these newly synthesized abnormal samples, both with  $256 \times 256$  pixels. In the context of Section 2.2, take any  $X \in \mathcal{X}$ , if  $X$  is one of the original images then the corresponding  $Y$  should be itself, that is,  $Y = X$ ; if  $X$  is one of the synthesized abnormal images, then the corresponding  $Y$  is its original image. Figure 3 is an example of the synthesized abnormal samples during data pre-processing. Figure 3a is the original image captured from a test line and Figure 3b is the corresponding synthesized abnormal sample after pasting abnormal objects (e.g. nails) onto the original image; the abnormal regions on the synthesized image are marked by red arrows on Figure 3c.

**Algorithm.** Our Algorithm 1 of anomaly detection for railway inspection is divided into two steps: the meta-learning step and the line-specific anomaly detection step.

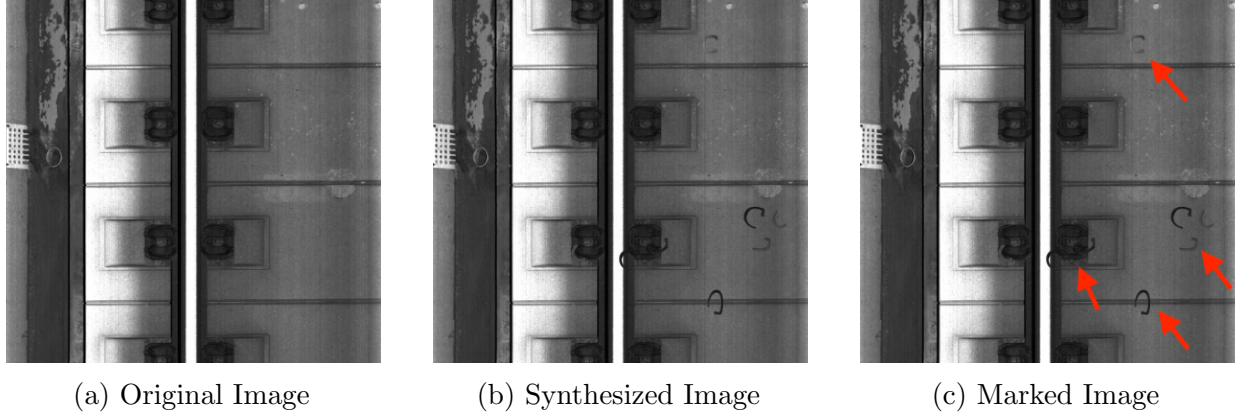


Figure 3: Example of Synthesized Abnormal Sample

In step one (the meta-learning step), for each rail line, we train the model described in Equations (6) and (8) through the pre-processed data and find the optimal parameters  $\omega_G$  and  $\omega_D$  for two neural networks  $G_{\omega_G}$  and  $D_{\omega_D}$  respectively. We use such optimal parameters as the meta knowledge for the anomaly reconstruction in each rail line.

In step two (the line-specific anomaly detection step), for each task-specific problem, we divide the input image  $X$  and reconstructed image  $\hat{X} = G_{\omega_G}(X, Z)$  into  $16 \times 16$  blocks  $(X_{kl}, \hat{X}_{kl})$  for  $k, l = 1, \dots, 16$ , and compute the SSIM loss for each block pair  $(X_{kl}, \hat{X}_{kl})$ . We pick three block pairs  $(X_{(j)}, \hat{X}_{(j)})$  for  $j = 1, 2, 3$  with the three lowest SSIM values, and compute the difference  $\Delta X_{(j)} = X_{(j)}^i - \hat{X}_{(j)}$ . For experiments with limited labeled data, the label for  $X$  is given. In the deployment stage without labeled data,  $X$  is labeled as *abnormal* if the lowest block SSIM loss is less than a predetermined threshold  $\mu_0 > 0$ . As described in Equation (8), a binary classifier is trained with input  $(\Delta X_{(1)}, \Delta X_{(2)}, \Delta X_{(3)})$ .

**Computing resources.** We utilize a workstation with a single Nvidia GeForce GTX 1080 GPU, an Intel Core i7-7700K CPU and 16GB memory for all experiments.

**Performance evaluation.** The experiment consists of two stages. In the first stage, we train our meta-learning framework with 100 known anomaly samples; and in the second stage, with 50 known anomaly samples. This experiment is to test the accuracy and the robustness of our meta-learning framework.

We consider five indicators to measure the performance of anomaly detection: the confirmed anomalies, the confirmed anomalies in official anomaly record, the missed anomalies in official anomaly record, the newly-discovered anomalies besides official anomaly record and the percentage of newly-detected anomalies. As a reference,

- *Confirmed Anomalies* refers to the number of anomaly samples detected by our meta-learning framework and confirmed by operation staff.
- *Confirmed Anomalies in Official Anomaly Records* refers to the number of anomaly samples in the Official Anomaly Records that are detected by our meta-learning

---

**Algorithm 1** Meta-Learning Algorithm for Anomaly Detection
 

---

**Input:** Hyper-parameters learning rate  $\alpha$ ,  $\beta$ ,  $\gamma$

Initialize the network parameter  $\omega = (\omega_G, \omega_D)$  of  $G_{\omega_G}, D_{\omega_D}$

```

1:
2: STEP ONE: META-LEARNING STEP
3: while not converged (or epoch < 300 ) do
4:   Sample a batch of lines  $\{L_i\}_{i=1}^N$ 
5:   for each  $L_i$  do
6:     Construct task  $T_i$  including training set, validation set for each line  $T_i = (D_i^{tr}, D_i^{val})$  from  $L_i$ 
7:     Evaluate the gradient for  $\omega_G$ ,  $\nabla_{\omega_G} L_{T_i}(\omega; D_i^{tr})$ , where
8:      $L_{T_i}(\omega; D_i^{tr}) = \sum_{(X_j, Y_j) \in D_i^{tr}} \mathcal{L}_{\text{meta}}(G_{\omega_G}, D_{\omega_D}) = \sum_{(X_j, Y_j) \in D_i^{tr}} [V_{\text{GAN}}(G_{\omega_G}, D_{\omega_D}) + w_1 V_{L_2}(G_{\omega_G}) - w_2 V_{\text{SSIM}}(G_{\omega_G})]$ 
9:     Update  $\omega_G$ :  $\omega_G \leftarrow \omega_G - \alpha \nabla_{\omega_G} L_{T_i}(\omega_G, \omega_D; D_i^{tr})$ 
10:   end for
11:   Evaluate the gradient for  $\omega_D$ ,  $\nabla_{\omega_D} L_{T_i}(\omega; D_i^{val})$ , where
12:    $L_{T_i}(\omega; D_i^{val}) = \sum_{(X_j, Y_j) \in D_i^{val}} \mathcal{L}_{\text{meta}}(G_{\omega_G}, D_{\omega_D}) = \sum_{(X_j, Y_j) \in D_i^{val}} [V_{\text{GAN}}(G_{\omega_G}, D_{\omega_D}) + w_1 V_{L_2}(G_{\omega_G}) - w_2 V_{\text{SSIM}}(G_{\omega_G})]$ 
13:   Update  $\omega_D$ :  $\omega_D \leftarrow \omega_D - \beta \sum_{i=1}^N \nabla_{\omega_D} L_{T_i}(\omega; D_i^{val})$ 
14: end while
15:
16: STEP TWO: LINE-SPECIFIC ANOMALY DETECTION STEP
17: for each line  $L_i$  do
18:   Construct meta-test set  $D_i^{test}$  for line  $L_i$  and update  $\omega_G$  again:  $\omega_{G_i} \leftarrow \omega_G - \alpha \nabla_{\omega_G} L_{T_i}(\omega; D_i^{test})$ , where
19:    $L_{T_i}(\omega; D_i^{test}) = \sum_{(X_j, Y_j) \in D_i^{test}} \mathcal{L}_{\text{meta}}(G_{\omega_G}, D_{\omega_D}) = \sum_{(X_j, Y_j) \in D_i^{test}} [V_{\text{GAN}}(G_{\omega_G}, D_{\omega_D}) + w_1 V_{L_2}(G_{\omega_G}) - w_2 V_{\text{SSIM}}(G_{\omega_G})]$ 
20:   for each sample  $X^i$  do
21:     Construct corresponding corrected sample  $\hat{X}^i(\omega_{G_i}) = G_{\omega_{G_i}}(X^i, Z)$  and divide them into  $16 \times 16$  blocks  $(X_{kl}^i, \hat{X}_{kl}^i(\omega_{G_i}))_{16 \times 16}$ 
22:     Calculate the block SSIM losses for  $(X_{kl}^i, \hat{X}_{kl}^i(\omega_{G_i}))$ 's,  $L_{\text{SSIM}}^{1,1,1}(X_{kl}^i, \hat{X}_{kl}^i(\omega_{G_i}))$  according to equation (5)
23:     Select three blocks  $(X_{(j)}^i, \hat{X}_{(j)}^i(\omega_{G_i}))$  for  $j = 1, 2, 3$  with the lowest SSIM values and calculate the differences,  $\Delta X_{(j)}^i(\omega_{G_i}) = X_{(j)}^i - \hat{X}_{(j)}^i(\omega_{G_i})$ 
24:     If the lowest block SSIM loss  $L_{\text{SSIM}}^{1,1,1}(X_{(1)}^i, \hat{X}_{kl}^i(\omega_{(1)})) \geq \mu_0$ , then  $\mathbf{1}_{X^i\{\text{normal}\}} = 1$ ; otherwise,  $\mathbf{1}_{X^i\{\text{normal}\}} = 0$ 
25:   end for
26:   while not converged (or epoch < 300 ) do
27:     Sample a batch of labeled images for training binary classifier  $p_{\theta_i}$ 
28:     Evaluate the cross entropy of the binary classifier  $\mathcal{L}_i(\theta_i, \omega) = -\mathbb{E}_{X^i, Z} [\mathbf{1}_{X^i\{\text{normal}\}} p_{\theta_i}(\Delta X_{(1)}^i(\omega_{(1)}), \Delta X_{(2)}^i(\omega_{(1)}), \Delta X_{(3)}^i(\omega_{(1)})) + (1 - \mathbf{1}_{X^i\{\text{normal}\}}) [1 - p_{\theta_i}(\Delta X_{(1)}^i(\omega_{(1)}), \Delta X_{(2)}^i(\omega_{(1)}), \Delta X_{(3)}^i(\omega_{(1)}))]]$ 
29:     Evaluate the gradient of the binary classifier  $\nabla_{\theta_i} \mathcal{L}_i(\theta_i, \omega)$ 
30:     Update  $\theta_i$ :  $\theta_i \leftarrow \theta_i - \gamma \nabla_{\theta_i} \mathcal{L}_i(\theta_i, \omega)$ 
31:   end while
32:   Apply the binary classifier to predict other unlabeled blocks of this line  $\bar{Y}^i = p_{\theta_i}(X^i, G_{\omega_G}(X^i, Z))$ 
33: end for

```

---

framework and confirmed by operation staff.

- The *Missed Anomalies in Official Anomaly Records* refers to the number of anomaly samples in the Official Anomaly Records which are missed by our meta-learning framework.
- The *Newly-Discovered Anomalies* refers to the number of anomaly samples that are detected by our meta-learning framework and confirmed by operation staff, but were missing in the Official Anomaly Record.
- The *Percentage of Newly-Discovered Anomalies* refers to the *Newly-Discovered Anomalies* divided by the *Official Anomaly Record*

**Results.** The test results for these two stage of experiment are shown in Table 1a and Table 1b.

- Despite the limited known anomaly samples, our meta-learning framework rarely misses any anomalies that were previously detected by human inspectors, as Column E shows. In fact, after manual inspection, it is confirmed that all anomaly cases missed by our framework are due to internal structural changes which were not captured by images.
- Moreover, despite the reduction in the number of labeled samples from 100 to 50, comparing the detected number of anomaly cases between Column D in Table 1a and Column D in Table 1b for all rail lines shows the robustness of our meta-learning framework for anomaly detection.
- In spite of limited known anomaly samples, our meta-learning framework can detect significantly more, in fact several time more anomalies than by human inspectors, as indicated in Column G of Table 1a and Table 1b.

## 5 Deployment and Performance

The robustness and high accuracy of our framework leads to its deployment to the high-speed rail inspection system. Since 2021 this system has been deployed in the following high-speed railways of China: the Beijing–Shanghai line, the Beijing–Harbin line, the Beijing–Guangzhou line, the Lanzhou–Xinjiang line, and the Yichang–Wanzhou line.

The entire inspection system consists of three components: comprehensive track inspection vehicles, the cloud-based storage and processing system, and the client-based operating system. The comprehensive track inspection vehicle is a four-axle inspection vehicle and adopts a dual power transmission system. It uses charged-coupled device cameras to collect high-definition images of the track in real time during vehicle operation and records the corresponding position data. The power of the vehicle is  $2 \times 353\text{kW}$ , and the running speed is 160 km/h. On average, 1000 images are captured for every kilometer, and the resolution of each picture is about  $5120 \times 5120$ . Collected images are sent to the cloud-based storage and processing system in real time through the wireless network. As part of operation trials, our meta-learning

Table 1: Experiment Results with Limited Labeled Samples

(a) With 100 Labeled Samples

	Total Num- ber of Images (A)	Official Anomaly Record (B)	Confirmed Anoma- lies (C)	Confirmed Anoma- lies in Official Record (D)	Missed Anoma- lies in Official Record (E)	Newly De- tected Anoma- lies (F)	Percentage of Newly De- tected Anoma- lies (G)
<b>Test Line 1</b>	173702	12	83	12	0	71	591%
<b>Test Line 2</b>	103302	1	14	1	0	13	1300%
<b>Test Line 3</b>	149054	7	56	7	0	49	700%
<b>Test Line 4</b>	104250	26	112	26	0	86	330%
<b>Test Line 5</b>	168666	34	752	34	0	718	2111%

(b) With 50 Labeled Samples

	Total Num- ber of Images (A)	Official Anomaly Record (B)	Confirmed Anoma- lies (C)	Confirmed Anoma- lies in Official Record (D)	Missed Anoma- lies in Official Record (E)	Newly De- tected Anoma- lies (F)	Percentage of Newly De- tected Anoma- lies (G)
<b>Test Line 1</b>	173702	12	74	12	0	62	516%
<b>Test Line 2</b>	103302	1	3	1	0	2	200%
<b>Test Line 3</b>	149054	7	49	6	1	43	614%
<b>Test Line 4</b>	104250	26	61	25	1	36	138%
<b>Test Line 5</b>	168666	34	555	34	0	521	1532%

Table 2: Performance of Deployment in High-Speed Rail System

(a) Anomaly Detection Ability

	Total Number of Images	Official Anomaly Record	Detected Confirmed Anomalies	& Percentage of Newly De- tected Anoma- lies
Test Line 1	173702	12	38	230%
Test Line 2	103302	1	4	300%
Test Line 3	149054	7	21	250%
Test Line 4	104250	26	64	162%
Test Line 5	68666	34	414	1170%

(b) Workload Reduction

	Total Number of Im- ages	Detected Anomalies	Suspected	Workload Reduction
Test Line 1	173702	205		99.89%
Test Line 2	103302	16		99.98%
Test Line 3	149054	222		99.85%
Test Line 4	104250	119		99.89%
Test Line 5	68666	719		99.75%

(c) Time Reduction

	Total Number of Images	Estimated Time for Hu- man (Hours)	Estimated Time for Machine (Hours)	Time Reduction
Test Line 1	173702	1447.5	48.3	96.7%
Test Line 2	103302	860.9	28.7	96.7%
Test Line 3	149054	1242.1	41.4	96.7%
Test Line 4	104250	868.7	29.0	96.7%
Test Line 5	68666	1405.5	46.9	96.7%

framework is deployed in the cloud-based storage and processing system to analyze the collected images in real time. Suspicious anomalies reported by our system are sent to the client-based operating system, which are then sent to the maintenance personnel for review and double-checking to ensure safety for the train operation.

In the system, a threshold value  $\mu_0 = 0.95$  is adopted to determine that any blocks with SSIM value lower than the threshold are anomalies. Results of the deployment are reported in Table 2.

- Our meta-learning framework has managed to detect several times more new anomalies than human inspectors, without prior labeled data. It has learned the difference between foreign objects and background images, and has detected most foreign objects in each line (Table 2a).
- Our framework has reduced the workload of inspecting millions of images to simply double-checking only hundreds of detected images, over 99.7% workload reduction (Table 2b).
- Using our framework, it takes less than two days for anomaly detection, instead of several months of inspection, with over 96% time saved (Table 2c).

## 6 Conclusion

In this work, we propose a deep learning framework for anomaly detection: meta-learning with incorporation of GANs and SSIMs. Our framework has been deployed in the high-speed rail inspection system in China since 2021. Its superb performance demonstrates that our meta-learning framework is promising for general anomaly detection tasks: it is sharp and robust in identifying anomalies and capable of significantly reducing workload.

## References

- [1] Martin Arjovsky, Soumith Chintala, and Léon Bottou. Wasserstein generative adversarial networks. In *International Conference on Machine Learning*, pages 214–223. PMLR, 2017.
- [2] Haoyang Cao and Xin Guo. Generative adversarial network: some analytical perspectives. In *Machine Learning And Data Sciences For Financial Markets: A Guide To Contemporary Practices*, pages 493–518. Cambridge University Press, 2022.
- [3] Varun Chandola, Arindam Banerjee, and Vipin Kumar. Anomaly detection: A survey. *ACM Computing Surveys (CSUR)*, 41(3):1–58, 2009.
- [4] Haoqing Cheng, Heng Liu, Fei Gao, and Zhuo Chen. ADGAN: A scalable GAN-based architecture for image anomaly detection. In *2020 IEEE 4th Information Technology, Networking, Electronic and Automation Control Conference (ITNEC)*, volume 1, pages 987–993. IEEE, 2020.

- [5] Dan Chianucci and Andreas Savakis. Unsupervised change detection using spatial transformer networks. pages 1–5, 2016.
- [6] Emily L Denton, Soumith Chintala, Arthur Szlam, and Rob Fergus. Deep generative image models using a Laplacian pyramid of adversarial networks. In *Advances in Neural Information Processing Systems*, pages 1486–1494, 2015.
- [7] Hao Feng, Zhiguo Jiang, Fengying Xie, Ping Yang, Jun Shi, and Long Chen. Automatic fastener classification and defect detection in vision-based railway inspection systems. *IEEE Transactions on Instrumentation and Measurement*, 63(4):877–888, 2013.
- [8] Chelsea Finn, Aravind Rajeswaran, Sham Kakade, and Sergey Levine. Online meta-learning. In *International Conference on Machine Learning*, pages 1920–1930. PMLR, 2019.
- [9] Chelsea Finn, Kelvin Xu, and Sergey Levine. Probabilistic model-agnostic meta-learning. *Advances in Neural Information Processing Systems*, 31, 2018.
- [10] Arnab Ghosh, Viveka Kulharia, Amitabha Mukerjee, Vinay Namboodiri, and Mohit Bansal. Contextual RNN-GANs for abstract reasoning diagram generation. *arXiv preprint arXiv:1609.09444*, 2016.
- [11] Xavier Giben, Vishal M Patel, and Rama Chellappa. Material classification and semantic segmentation of railway track images with deep convolutional neural networks. In *2015 IEEE International Conference on Image Processing (ICIP)*, pages 621–625. IEEE, 2015.
- [12] Xavier Gibert, Vishal M Patel, and Rama Chellappa. Robust fastener detection for autonomous visual railway track inspection. In *2015 IEEE Winter Conference on Applications of Computer Vision*, pages 694–701. IEEE, 2015.
- [13] Ian J. Goodfellow, Jean Pouget-Abadie, Mehdi Mirza, Bing Xu, David Warde-Farley, Sherjil Ozair, Aaron Courville, and Yoshua Bengio. Generative adversarial nets. In *International Conference on Neural Information Processing Systems*, pages 2672–2680, 2014.
- [14] Xin Guo, Johnny Hong, Tianyi Lin, and Nan Yang. Relaxed Wasserstein with applications to GANs. In *ICASSP 2021-2021 IEEE International Conference on Acoustics, Speech and Signal Processing (ICASSP)*, pages 3325–3329. IEEE, 2021.
- [15] Geoffrey Hinton, Li Deng, Dong Yu, George E Dahl, Abdel-rahman Mohamed, Navdeep Jaitly, Andrew Senior, Vincent Vanhoucke, Patrick Nguyen, Tara N Sainath, et al. Deep neural networks for acoustic modeling in speech recognition: The shared views of four research groups. *IEEE Signal Processing Magazine*, 29(6):82–97, 2012.
- [16] Geoffrey E Hinton and Ruslan R Salakhutdinov. Reducing the dimensionality of data with neural networks. *science*, 313(5786):504–507, 2006.
- [17] S Hochreiter and J Schmidhuber. Long short-term memory. *Neural Computation*, 9(8):1735–1780, 1997.



- [18] Timothy Hospedales, Antreas Antoniou, Paul Micaelli, and Amos Storkey. Meta-learning in neural networks: A survey. *arXiv preprint arXiv:2004.05439*, 2020.
- [19] Gaoqiang Kang, Shibin Gao, Long Yu, and Dongkai Zhang. Deep architecture for high-speed railway insulator surface defect detection: Denoising autoencoder with multitask learning. *IEEE Transactions on Instrumentation and Measurement*, 68(8):2679–2690, 2018.
- [20] Alex Krizhevsky, Ilya Sutskever, and Geoffrey E Hinton. Imagenet classification with deep convolutional neural networks. In F. Pereira, C. J. C. Burges, L. Bottou, and K. Q. Weinberger, editors, *Advances in Neural Information Processing Systems*, volume 25. Curran Associates, Inc., 2012.
- [21] Wei-Sheng Lai, Jia-Bin Huang, Zhe Hu, Narendra Ahuja, and Ming-Hsuan Yang. A comparative study for single image blind deblurring. In *Proceedings of the IEEE Conference on Computer Vision and Pattern Recognition*, pages 1701–1709, 2016.
- [22] Yann LeCun, Patrick Haffner, Léon Bottou, and Yoshua Bengio. Object recognition with gradient-based learning. In *Shape, Contour and Grouping in Computer Vision*, 1999.
- [23] Chuan Li and Michael Wand. Precomputed real-time texture synthesis with markovian generative adversarial networks. In *European Conference on Computer Vision*, pages 702–716. Springer, 2016.
- [24] Yiwei Lu, Frank Yu, Mahesh Kumar Krishna Reddy, and Yang Wang. Few-shot scene-adaptive anomaly detection. In *European Conference on Computer Vision*, pages 125–141. Springer, 2020.
- [25] Pauline Luc, Camille Couprie, Soumith Chintala, and Jakob Verbeek. Semantic segmentation using adversarial networks. *arXiv preprint arXiv:1611.08408*, 2016.
- [26] Fiete Lürer, Dominik Mautz, and Christian Böhm. Anomaly detection in time series using generative adversarial networks. In *2019 International Conference on Data Mining Workshops (ICDMW)*, pages 1047–1048. IEEE, 2019.
- [27] Alireza Makhzani, Jonathon Shlens, Navdeep Jaitly, and Ian Goodfellow. encoders. In *International Conference on Learning Representations*, 2016.
- [28] Sebastian Nowozin, Botond Cseke, and Ryota Tomioka. f-GAN: Training generative neural samplers using variational divergence minimization. *Advances in Neural Information Processing Systems*, 29, 2016.
- [29] Deepak Pathak, Philipp Krahenbuhl, Jeff Donahue, Trevor Darrell, and Alexei A Efros. Context encoders: Feature learning by inpainting. In *Proceedings of the IEEE conference on computer vision and pattern recognition*, pages 2536–2544, 2016.
- [30] Xuebin Qin, Zichen Zhang, Chenyang Huang, Chao Gao, Masood Dehghan, and Martin Jagersand. Basnet: Boundary-aware salient object detection. In *Proceedings of the IEEE/CVF Conference on Computer Vision and Pattern Recognition*, pages 7479–7489, 2019.

- [31] Alec Radford, Luke Metz, and Soumith Chintala. Unsupervised representation learning with deep convolutional generative adversarial networks. *arXiv preprint arXiv:1511.06434*, 2015.
- [32] Scott Reed, Zeynep Akata, Xinchun Yan, Lajanugen Logeswaran, Bernt Schiele, and Honglak Lee. Generative adversarial text to image synthesis. *arXiv preprint arXiv:1605.05396*, 2016.
- [33] Olaf Ronneberger, Philipp Fischer, and Thomas Brox. U-net: Convolutional networks for biomedical image segmentation. In *International Conference on Medical Image Computing and Computer-Assisted Intervention*, pages 234–241. Springer, 2015.
- [34] Andrei A. Rusu, Dushyant Rao, Jakub Sygnowski, Oriol Vinyals, Razvan Pascanu, Simon Osindero, and Raia Hadsell. Meta-learning with latent embedding optimization. In *International Conference on Learning Representations*, 2019.
- [35] Adam Santoro, Sergey Bartunov, Matthew Botvinick, Daan Wierstra, and Timothy Lillicrap. Meta-learning with memory-augmented neural networks. In *International Conference on Machine Learning*, pages 1842–1850. PMLR, 2016.
- [36] Thomas Schlegl, Philipp Seeböck, Sebastian M Waldstein, Georg Langs, and Ursula Schmidt-Erfurth. F-AnoGAN: Fast unsupervised anomaly detection with generative adversarial networks. *Medical Image Analysis*, 54:30–44, 2019.
- [37] Nitish Srivastava, Geoffrey Hinton, Alex Krizhevsky, Ilya Sutskever, and Ruslan Salakhutdinov. Dropout: A simple way to prevent neural networks from overfitting. *Journal of Machine Learning Research*, 15(56):1929–1958, 2014.
- [38] Pang-Ning Tan, Michael Steinbach, and Vipin Kumar. Introduction to data mining. 2016.
- [39] Carl Vondrick, Hamed Pirsiavash, and Antonio Torralba. Generating videos with scene dynamics. In *Advances in Neural Information Processing Systems*, pages 613–621, 2016.
- [40] Jacob Walker, Carl Doersch, Abhinav Gupta, and Martial Hebert. An uncertain future: Forecasting from static images using variational autoencoders. In *European Conference on Computer Vision*, pages 835–851. Springer, 2016.
- [41] Zhou Wang, Alan C Bovik, Hamid R Sheikh, and Eero P Simoncelli. Image quality assessment: from error visibility to structural similarity. *IEEE transactions on image processing*, 13(4):600–612, 2004.
- [42] Zhou Wang, Alan C Bovik, Hamid R Sheikh, and Eero P Simoncelli. Image quality assessment: from error visibility to structural similarity. *IEEE transactions on image processing*, 13(4):600–612, 2004.
- [43] Jhih-Ciang Wu, Ding-Jie Chen, Chiou-Shann Fuh, and Tyng-Luh Liu. Learning unsupervised metaformer for anomaly detection. In *Proceedings of the IEEE/CVF International Conference on Computer Vision*, pages 4369–4378, 2021.

- [44] Chih-Yuan Yang, Chao Ma, and Ming-Hsuan Yang. Single-image super-resolution: A benchmark. pages 372–386, 2014.
- [45] Vitjan Zavrtanik, Matej Kristan, and Danijel Skočaj. Reconstruction by inpainting for visual anomaly detection. *Pattern Recognition*, 112:107706, 2021.
- [46] Shen Zhang, Fei Ye, Bingnan Wang, and Thomas G. Habetler. Few-shot bearing anomaly detection via model-agnostic meta-learning. In *2020 23rd International Conference on Electrical Machines and Systems (ICEMS)*, pages 1341–1346, 2020.